DESY Summer Student
Programme 2011

Impact of the geomagnetic field on the angular resolution of Imaging Atmospheric Cherenkov Telescopes

CTA

Alma Mater Studiorum - University of Bologna

Author: Lucia Ambrogi **Supervisor: Serguei Vorobiov**

Abstract

The Cherenkov Telescope Array (CTA) will be a ground-based gamma-ray observatory which will study astrophysical sources in the energy range from 10 GeV to about 100 TeV. CTA will detect these very-high energy gamma-rays by measuring the γ-ray induced particle showers in the atmosphere and exploiting an array of a few tens of Imaging Atmospheric Cherenkov Telescopes (IACTs). Due to the presence of the Earth's magnetic field which systematically deflects charged particles in the shower, the Cherenkov light images in the camera of an IACT are rotated and modified in photon density. This phenomenon affects the sensitivity of the telescopes. The aim of this work is to evaluate the impact of the geomagnetic field on the angular resolution of the telescopes.

1 Very High Energy gamma-ray astronomy

Observations of electromagnetic radiation in TeV energy range are a sensitive probe of the highest energy physical processes occurring in a variety of astrophysical objects. They allow us to measure the properties of energetic particles in the Universe, such as the details of their acceleration processes, composition and energy spectra. TeV gamma rays provide a large window into the non-thermal Universe, which is complementary to the other wavelength domains. This *very high energy* (VHE, $E \gtrsim 10\ GeV$) domain, is also important for probing fundamental physics. The mass scale for cold dark matter particle candidates is expected for example in this energy range.

Charge particles travelling in the Universe are deflected by cosmic magnetic fields, while neutral particles (as photons or neutrinos) are not. Hence, the VHE γ-rays point back to the location of their origin and carry information about their production sites.

The first detected VHE γ-ray source is the Crab Nebula (Weekes et al. 1989); it is a pulsar wind nebula (PWN) which served, due to its strong and stable flux at TeV, to cross-check the detection and analysis techniques. During the last decade the current generation experiments with improved sensitivity, like H.E.S.S. MAGIC and VERITAS, detected and studied more than 100 γ-emitting objects of varius types. There are galactic sources, like supernova remnants (SNR), microquasar, pulsar and PWN, and extra-galactic sources (active galactic nuclei (AGN) of various types, mostly blazars) [2].

The rapidly decreasing spectra of cosmic accelerators[1] present a natural upper limit to the highest energy observed γ-rays (currently $\sim 100\ TeV$). At PeV ($\equiv 10^{15}\ eV$) or energies, the γ-rays are absorbed by the low-energy CMB photons and their free path ($\sim 7\ kpc$) becomes smaller than the Galaxy diameter ($\sim 30\ kpc$).

2 Imaging Atmospheric Cherenkov Detection Technique

2.1 Cherenkov Radiation of EM Shower

When a high energy γ-ray enters the atmosphere it dissipates its energy through the creation of an electron-positron pair. These particles in turn dissipate their energy through the bremsstrahlung (or "braking-radiation") process in the Coulomb field of the nuclei that comprise the atmosphere. The combined effect of pair production and bremsstrahlung emission by HE photons and electrons results in the formation of an *electromagnetic shower*. New generations of particles become involved into these processes, which leads to an exponential growth in the number of particles as a function of the depth traversed

[1] The CR power-law spectrum is $dN \sim E^{-2} dE$.

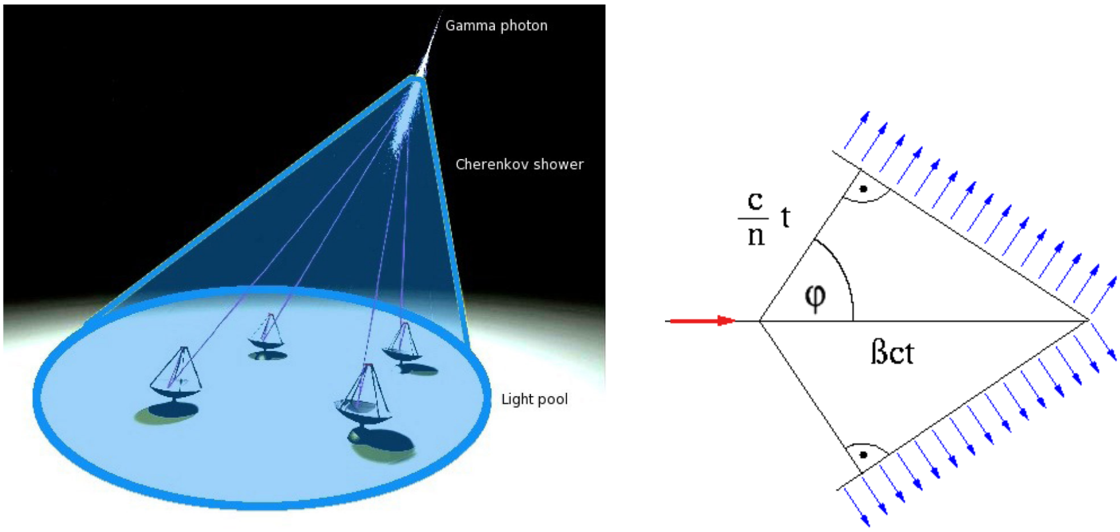

(a) (b)

Figure 1: (a) Production of an Electromagnetic Extensive Air Shower. (b) Schematic picture of the Cherenkov radiation emitted by a charged particle.

through the atmosphere. The energy of the $e^+ - e^-$ pairs finally drops below the critical energy E_c ($E_c \sim 85\ MeV$ in air [8]). At this point, the $e^+ - e^-$ pairs will preferentially lose their energy via atomic collision (ionization and excitation processes) rather than bremsstrahlung emission, thus leading to the absorbition of the shower.

A simple model can be used to describe the mean number of particles produced and their mean energies as a function of the penetration depth x in the material. It is convenient to introduce the scale variables $t = x/X_0$, where X_0 is the characteristic *radiation length*[2] of the medium; in air $X_0 = 36.6\ g/cm^2$. In this way the distance is measured in units of radiation length and, after t radiation lengths, the number N of particles (i.e., photons, e^+ and e^-) in the shower and the energy $E(t)$ carried by each of them, can be roughly approximated by:

$$N = 2^t \qquad\qquad E(t) = E_0/2^t, \tag{1}$$

where E_0 is the energy of the primary photon (or γ-ray) that initiated the shower.

This simplistic model describes correctly the behavior of real showers, in which the number of particles at the shower maximum $N_{max} \sim E_0/E_c$. The maximum penetration depth t_{max} is proportional to the logaritmic ratio between the primary energy and the critical energy, i.e. $t_{max} \propto ln(E_0/E_c)$.

The charged particles that comprise the shower (i.e., electrons and positrons) travel relativistically through the atmosphere. When a charged particle moves in a medium with velocity βc greater than the phase velocity of the light c/n in the same medium (where n is the refraction index of the medium and c is the speed of light in vacuum), a light is emitted. This radiation is called *Cherenkov radiation*. The condition to get Cherenkov radiation is: $\beta c > c/n \Rightarrow \beta > 1/n$ (see figure 1). This requirement sets a threshold energy for the emission of Cherenkov light that depends on the value of the refraction index: $E_{thr} = m\sqrt{1 - 1/n^2}$, where m is the particle mass. At sea level, the refraction index in the air is $n = 1.0003$ [5] and the Cherenkov threshold energy for electrons is

[2] At 1 radiation length, bremsstrahlung photon loses all but $1/e$ of its energy and it is also 7/9 of the mean free path for the pair production process.

$E_{thr} \sim 21\ MeV$. When $E \geq E_{thr}$ an electromagnetic wave is created. The coherent wavefront formed is conical in shape and is emitted at an angle θ_c given by:

$$cos\ \theta_c = \frac{1}{\beta n} \tag{2}$$

with respect to the particle trajectory [4].

The number of photons per unit path length of a particle with charge ze and per unit photon energy interval is:

$$\frac{d^2N}{dxdE} = \frac{\alpha z^2}{\hbar c} sin^2(\theta_c) \approx 370\ sin^2(\theta_c) \quad eV^{-1}cm^{-1}(z = 1). \tag{3}$$

This is the so-called *Frank-Tamm formula* [1].

The Cherenkov emission in the shower is used to detect primary HE photons.

2.2 Imaging Atmospheric Cherenkov Technique

Given the very low fluxes of γ-rays in the VHE regime[3], direct detection from balloons or satellites is excluded.

Above $\sim 10\ GeV$ it becomes possible to detect indirectly HE photons by means of γ-induced particles cascades.

Imaging Atmospheric Cherenkov Telescopes (IACTs) use focusing mirrors to image the Cherenkov light emitted by the shower particles onto a *camera* of ~ 1000 pixels consisting of individual photo-detectors. This high-resolution camera typically consists of an array of photomultiplier tubes (PMTs), placed in the focal plane of the mirror and sampling the Cherenkov image of *Extensive Air Showers* (EAS). The smaller the pixel size (the larger the number of PMTs), the finer is the imaging.

The detection of γ-ray shower has to compete with hadronic showers from charged *cosmic rays* (CR), that have higher flux ($\Phi_{had} \sim 1000\ \Phi_{EM}$). However, development of hadronic-induced shower allow to efficiently suppress the hadronic background. The secondary particles in hadronic interactions have average transverse momentum $p_\perp$ of more than 300 MeV/c. The transverse momenta in electromagnetic interactions are of the order of m_e, i.e. ~ 1000 times lower [5]. For this reason hadronic showers, and hence their images, are irregular while the electromagnetic ones are smooth and compact. In fact, in contrast to the well-collimated electromagnetic air-showers induced by γ-rays (or electrons), air-showers induced by CR nucleons typically are more spread and characterized by a number of electromagnetic sub-shower induced by π^0 decays.

Another difference comes from the effect of perspective when an array of IACTs is pointing at a potential point-like γ-ray source. The axes of images of the γ-induced shower coming from the direction of the source intersect near the source position, while the background images are randomly oriented in the camera.

Rejection of the background is thus a very important performance criterion for γ-ray detectors. It is achieved on the basis of shower shape and direction. Currently, IACT arrays reach background rejection both at the hardware (trigger) level rejecting the 'diffuse' images of CR showers and the *night-sky background* (NSB) fake images, and at the software level, based on the analysis of image parameters[4] (e.g. the mean shower width and direction) [3].

[3]Flux of VHE γ-rays: $O(10^{-11})$ photons per cm^{-2}-sec for souces above 1 TeV [2]

[4]Advancements in the Cherenkov imaging technique occured in 1990s, after A.M. Hillas outlined the differences in the development of EM and hadronic showers and their Cherenkov images.

The current generation of IACT experiments use multiple telescopes for two main reasons: (a) to image the air-shower from different viewing angles for improved reconstruction of γ-ray direction and rejection of CR background and (b) to apply a coincidence requirement rejecting single-telescope triggers [2].

Nevertheless, IACTs are optical devices and therefore can operate only on clear moonless nights and good weather.

3 Cherenkov Telescope Array

Cherenkov Telescope Array (CTA) will be a ground-based VHE gamma-ray observatory optimized for the energy range from 10 GeV to about 100 TeV.

The main goals of CTA are the understanding of the acceleration mechanisms of the particles in astrophysical objects as well as the study of the cosmic rays origin and their interactions, the investigation of the nature of dark-matter particles and the search for quantum gravity [12].

The facility will consist of several tens of Cherenkov telescopes, to be compared with H.E.S.S. MAGIC or VERITAS arrays, which use at most four telescopes. Such an array will allow the detection of γ-ray induced cascades over a larger area on the ground, increasing the number of detected gamma rays, and at the same time providing a much larger number of Cherenkov images of each cascade. This will result in both improved angular resolution and better suppression of the CR background events, and finally in a gain in sensitivity of the telescopes [11].

The observatory will consist of two arrays, one in the northern and the other in the southern hemisphere, ensuring a full sky coverage. Three different types of telescopes are envisaged in the southern hemisphere in order to cover the central part of the galactic plane and to observe mostly galactic sources. The sensitivity of the northern array will be optimized for extra-galactic objects (up to ~ 10 TeV).

The *Large Size Telescopes* (LST) with a diameter of about 24 m, spaced approximately 100 m apart, will cover the energy range from 10 GeV to 100 GeV. For events down to a few tens of GeV (low energy events) one needs a very large mirror area, in order to efficiently sample and detect the Cherenkov light. The fraction of area covered by mirrors should be of the order of $5-10\%$. Since event rates are high, the area of this part of the array can be relatively small (few times 10,000 square meters). The *Medium Size Telescopes* (MST) will have a diameter of12 m and they will cover the energy range from 100 GeV to about 10 TeV. This kind of telescopes will be a few tens. There will be also a few tens of *Small Size Telescopes* (SST) with a diameter of about 5 m, optimized for energies above 10 TeV. For those highest energy events, the main limitation is the low number of detected γ-ray showers, the array therefore needs to cover an area of many square kilometers for the best performance. Fortunately, at these energies the Cherenkov light yield is large and it means that the shower can be detected well beyond the 140 m radius of a typical Cherenkov light pool [11].

3.1 CTA Design Study: simulation and analysis tools

Monte Carlo simulations are used to generate particle shower and simulate the detector response, which allows to design detectors and understand their performances as well as to compare their potential. The performance of an IACT array such as CTA depends on a large number of technical parameters. The main tools used by the CTA collaboration, which we also employed in the presented study, are:

- **CORSIKA**: the program used to simulate EAS initiated by high energy cosmic radiation (primary photons is our case). It tracks particles through the atmosphere: interaction, annihilation, decays and production of secondary particles are taken into account. With the IACT option of CORSIKA we simulate the Cherenkov light hitting any configuration of telescopes. Each telescope is represented by a mirror area; if the Cherenkov light passes through it, the event is stored and can be used for the detector simulation. The deflection of charged shower particles due to the geomagnetic field is also calculated.

- **sim_telarray**: the package used to simulate the details of the IACT detector response. The experimental setup used in this work is an array of 9 large size telescopes on a regular grid spaced 80 m apart; each telescope has a diameter of 23 m and a pixel size of 0.09 deg [8].

- **EventDisplay**: the program we used for the event reconstruction: image cleaning, calculation of image parameters, reconstruction of the direction, energy, impact parameter, etc. of the shower. To use EventDisplay for CTA analysis, one first has to convert the simtel.gz file into ROOT format.

4 GEOMAGNETIC FIELD EFFECT

The Earth's magnetic field is approximately a magnetic dipole field variable in time and space. At any time and location, it is characterized by a direction and intensity. The corresponding Lorentz force (see formula 4) systematically deflects the charged particles in the EAS. The deviation from the original trajectory depends on the particles energies; according to the classical formulas:

$$\vec{F_L} = q\vec{v} \times \vec{B} \qquad R = \frac{p}{qB} \tag{4}$$

where q, v and p respectively are the charge, the velocity and the momentum of the particle and R is the radius of curvature.

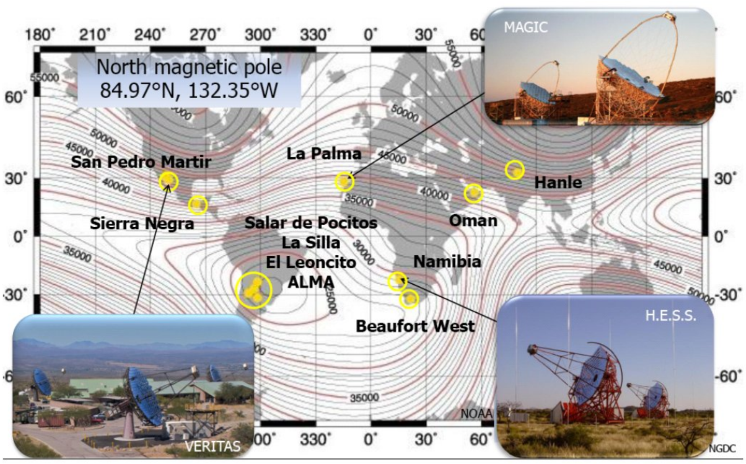

Figure 2: Isobars of total intensity - main field (in nT) measured by National Geophysical Data Center, including the position of candidate sites [8].

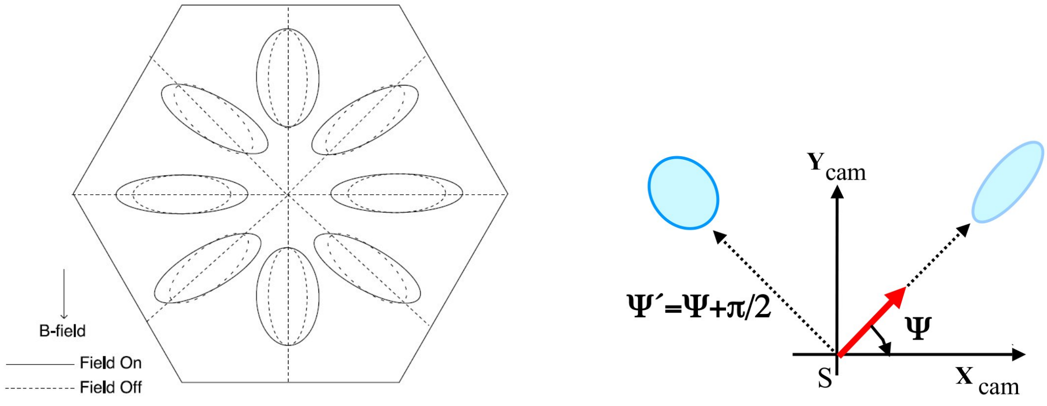

(a) (b)

Figure 3: (a) Effect of the geomagnetic field on the shape and orientation of images of VHE γ-rays. Undistorted γ-ray images are shown by the dotted curves; solid curves show the shape and orientation after distortion by the geomagnetic field [7]. (b) Geomagnetic effect for the images in the camera. The red vector represents the projection of Lorentz force in the camera and Ψ is the azimuth angle in the camera system.

In the case of EM shower the geomagnetic effect results in the east-west separation of electrons and positrons. For EAS developing at large angle with respect to the direction of the geomagnetic field, the corresponding Cherenkov light images in the camera of an IACT will be rotated and modified in size (see figure 4) which affects the angular and energy resolution of the IACTs and finally their sensitivity [6].

The two sites for the future CTA observatories are still under investigation. The picture 2 shows the isobars of the total intensity of the field and the position of some possible locations for CTA in both northern and southern hemispheres. In the table 1 some features of the sites are listed, i.e. latitudes, longitudes, elevations, declinations, horizonatal (H.I.) and vertical (V.I.) intensities.

Site	Latitude	Longitude	Elevation [m]	Declination	H.I. [μT]	V.I. [μT]
H.E.S.S. (Namibia)	23°16’18”S	16°30’00”E	1800	−13.62°	12.190	−25.684
El Leoncito (Argentina)	31°44’11”S	69°16’9”W	2600	0.7°	20.179	−12.529
La Palma (Spain)	28°45’42”N	17°53’26”E	2230	2.3°	31.635	26.749
San Pedro Martir (Mexico)	31°02’00”N	115°25’00”W	2800	11.30°	25.385	38.596

Table 1: Parameters of the candidate sites for CTA.

4.1 Main simulation parameters

In the simulations we worked with, the primary particles come from the following directions:

- **zenith angle** θ : 20° and 40°.
- **azimuth angle** ϕ : 0°→ particles arriving from north to the south, 90°→ from the

east to the west, 180°→ from the south to the north, and 270°→ from the west to the east.

The simulated VHE γ-ray source is located in the center of the camera. In this work we are interested in evaluating the geomagnetic field effect for point-like sources studied by the CTA Large Size Telescopes. We therefore studied the low energy events with the differential energy spectrum following the power law with a spectral index of -2.5 and extending up to the maximal energy $E_\gamma = 300\ GeV$. For such low energy events the deflection due to the magnetic field is stronger (see formula 4).

4.2 Geomagnetic modulation of the image parameters as a function of the azimuth in the camera

The *reconstructed azimuth angle* ϕ_{rec} in the camera system has been calculated starting from the knowledge of the *centroid*'s coordinates in the camera and actually it is the azimuth of the image centroid (in figure 4 it corresponds to the Ψ angle). The centroid of a given Cherenkov image is defined as the point corresponding to the mean value of light intensity.

We define α as the angle between the long axis of an image and the direction defined by the line connecting the image centre of gravity to the source position.

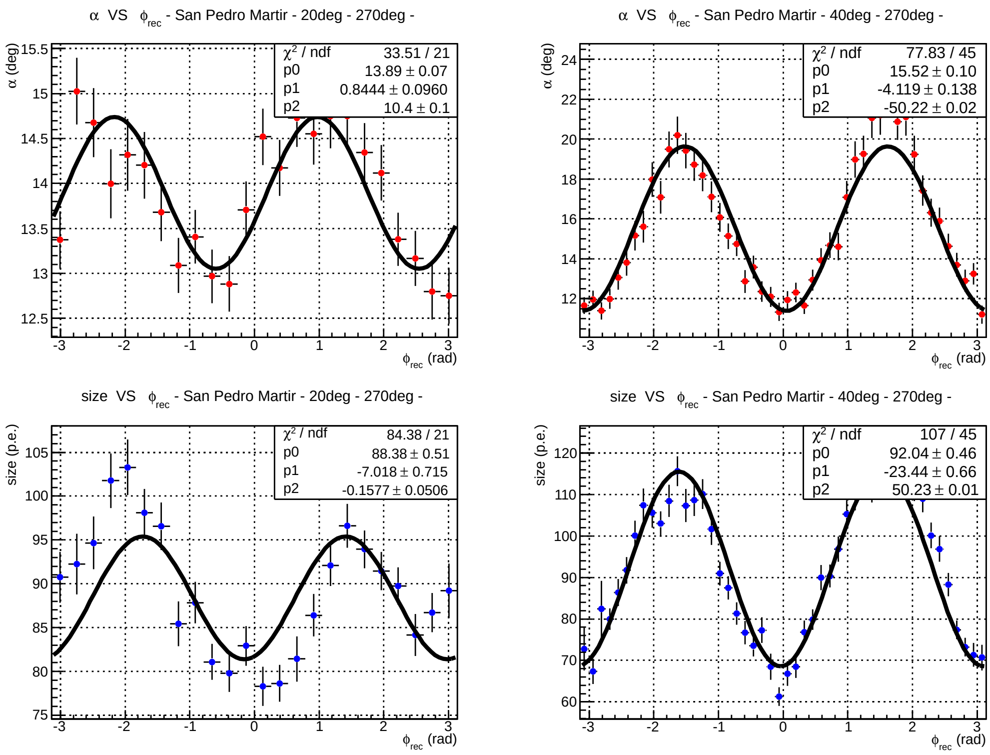

Figure 4: Modulation due to the geomagnetic field in the distribution of α angle (red markers) and image *size* (blue markers). Two different geographical zenith angles are shown: 20°(left side) and 40°(right side). The data used refer to the San Pedro Martir site, for a azimuth angle of 270°.

The mean value of this angle has been plotted as a function of ϕ_{rec} and it is shown in figure 4 (red markers).

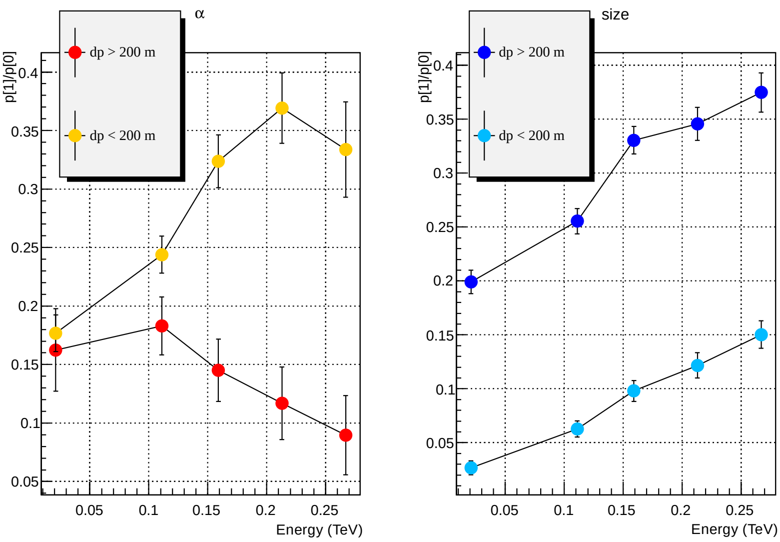

Figure 5: Amount of distortion due to the magnetic field estimated as the ratio between the *amplitude* $p[1]$ and the *average value* $p[0]$ of the distribution, as a function of the energy range. In each graph are shown separately the nearby events ($dp < 200\ m$) and the distant events ($dp > 200\ m$). The left plot shows the results for α-distribution, and the right plot the ones for *size*-distribution.

In the same picture is shown the distribution of the *size* (blue markers), defined as the amount of charge collected by the PMTs in the camera.

The two distributions, $\alpha = \alpha(\phi_{rec})$ and $size = size(\phi_{rec})$, have been calculated for two different zenith angles, 20°(left side) and 40°(right side), at the site of San Pedro Martir, where the intensity of the geomagnetic field is strongest. The geographical azimuth angle considered is 270°.

Taking into account the direction of the magnetic field's vector (oriented from the south to the north) and the one of the primary γ-ray propagation (oriented from west to east), it is easy to understand that the observed modulation is stronger for larger zenith angle since the Lorentz force is larger in that case. Indeed, the modulation amplitude is more important for 40°azimuth angle, while for the smaller angle the distribution is less regular.

In both cases the peak values are reached when the long axis of the image is perpendicular to the projection of the Lorentz force in the camera. When the long axis is orthogonal with respect to the projection of the force, the resulting image is wider due to the dispersion caused by the geomagnetic field. On the other hand, when the two directions are parallel, the image is much more elongated and it allows a better reconstruction of the source position (narrower α-distribution, see figure 4) [9].

The shape of the two distributions is very similar and is well fitted by a cosine modulation:

$$f(\phi_{rec}) \ = [p0] + [p1]\ cos\ (2\ (\phi_{rec} - [p2])). \tag{5}$$

The values of the parameters are shown in the figure.

To get these plots, we have applied several appropriate cuts. In particular, we considered two different ranges of *impact parameter dp*, which is defined as a distance between the shower axis and the telescope. The border between the two ranges for dp has been evaluated knowing that the mean light pool on the ground has radius about 140 m. Indeed, for showers arriving with an inclination of 40°, one obtains for the light-pool projection on the ground plane $dp \sim 200\ m$ [9].

The comparison of the essential image parameters between these two ranges shows that nearby and distant events are affected by the geomagnetic field in a different way. For $dp > 200\ m$ (distant events) the geomagnetic modulation of the image size is large, which significantly affects the energy resolution. On the contrary, when considering the angular resolution, it is clear from the example of α angle on figure 4 that the nearby events ($dp < 200\ m$) are the ones that are affected stronger.

These results are shown in figure 5. The amount of distortion due to the magnetic field is estimated as the ratio between the modulation *amplitude* $[p1]$ and the *average value* $p[0]$ as a function of energy. One can see that the *size* varies stronger for large impact parameter dp while the direction is most affected for the nearby events.

4.3 Angular resolution

With the stereoscopic approch it is possible to image the shower simultaneously by several telescopes detecting the same shower event. In the picture 6 is shown an example of a stereo event from in our analysis. Different colors of the images correspond to different telescopes detecting the same shower. The dark star represents the real source position, the pink star the reconstructed one.

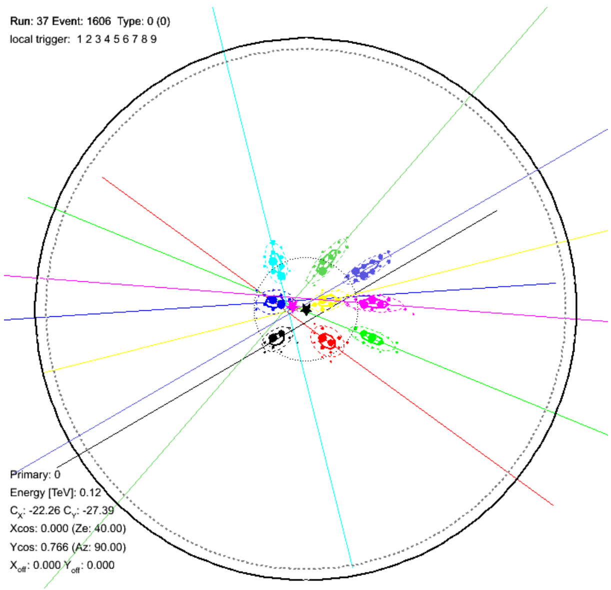

Figure 6: Example of stereo event used in CTA event analysis and display.

The quality of the reconstruced source position is characterized by the angular resolution of the telescopes.

The angular resolution is typically defined as the angle containing 68% of the distribution of the angles between the true and the reconstruced source positions, that is the quantity: $\sqrt{(x-\widetilde{x})^2 + (y-\widetilde{y})^2}$, where x and y are the real source coordinates in the camera system and $\widetilde{x}$ and $\widetilde{y}$ are the reconstructed ones.

Figure 7 shows the distributions of the reconstructed source position obtained using different cuts (varying mainly the cut in the image size), listed in the legend. The various angular resolutions are quoted in the table 2.

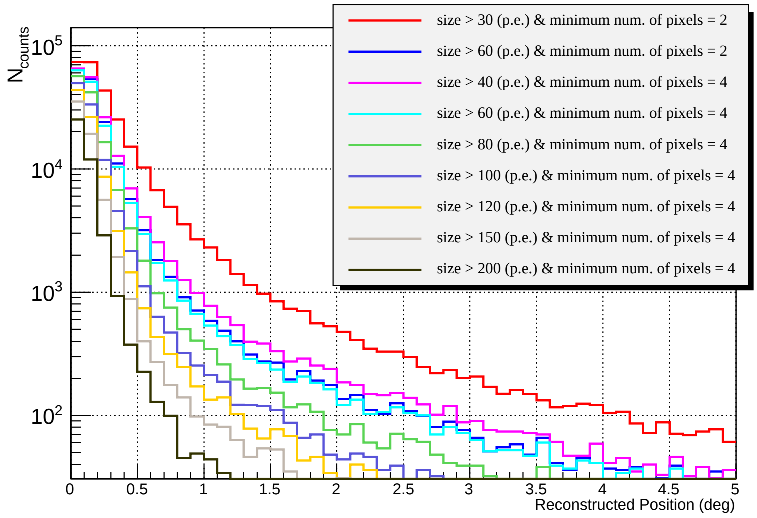

Figure 7: Distributions of the reconstructed source position obtained using different cuts listed in the legend.

CUT	Ang. Res. (°) at 68%	Ang. Res. (°) at 95%
Size > 30 (p.e.) and Minimum num. of pixels = 2	0.2977	1.3596
Size > 60 (p.e.) and Minimum num. of pixels = 2	0.1985	0.7382
Size > 40 (p.e.) and Minimum num. of pixels = 4	0.2155	0.8865
Size > 60 (p.e.) and Minimum num. of pixels = 4	0.1954	0.6539
Size > 80 (p.e.) and Minimum num. of pixels = 4	0.1722	0.5596
Size > 100 (p.e.) and Minimum num. of pixels = 4	0.1559	0.4775
Size > 120 (p.e.) and Minimum num. of pixels = 4	0.1446	0.4275
Size > 150 (p.e.) and Minimum num. of pixels = 4	0.1319	0.3720
Size > 200 (p.e.) and Minimum num. of pixels = 4	0.1180	0.3101

Table 2: Angular resolutions calculated at 68% and at 95% of the reconstruced position distribution for different cuts.

The best angular resolution corresponds to the stricter cuts in size because in that case the retained events contain in average more pixels and are therefore better defined.

To get the reconstructed source position, starting from individual images collected by each of the 9 telescopes, the modified weights method, described in [10], was used. It makes use of the following image parameters to weight the contribution of each image in order to reconstruct the source position and the shower core position:

- the angular distance between main axes of each couple of images;
- the size;
- the ratio *width*/*length*.

The *size* parameter corresponds to the sum of the pixel charges in the cleaned image[5], and *width* and *length* represent smaller and larger standard deviations of a two-dimensional Gaussian which fits at best the charges distribution in the cleaned image.

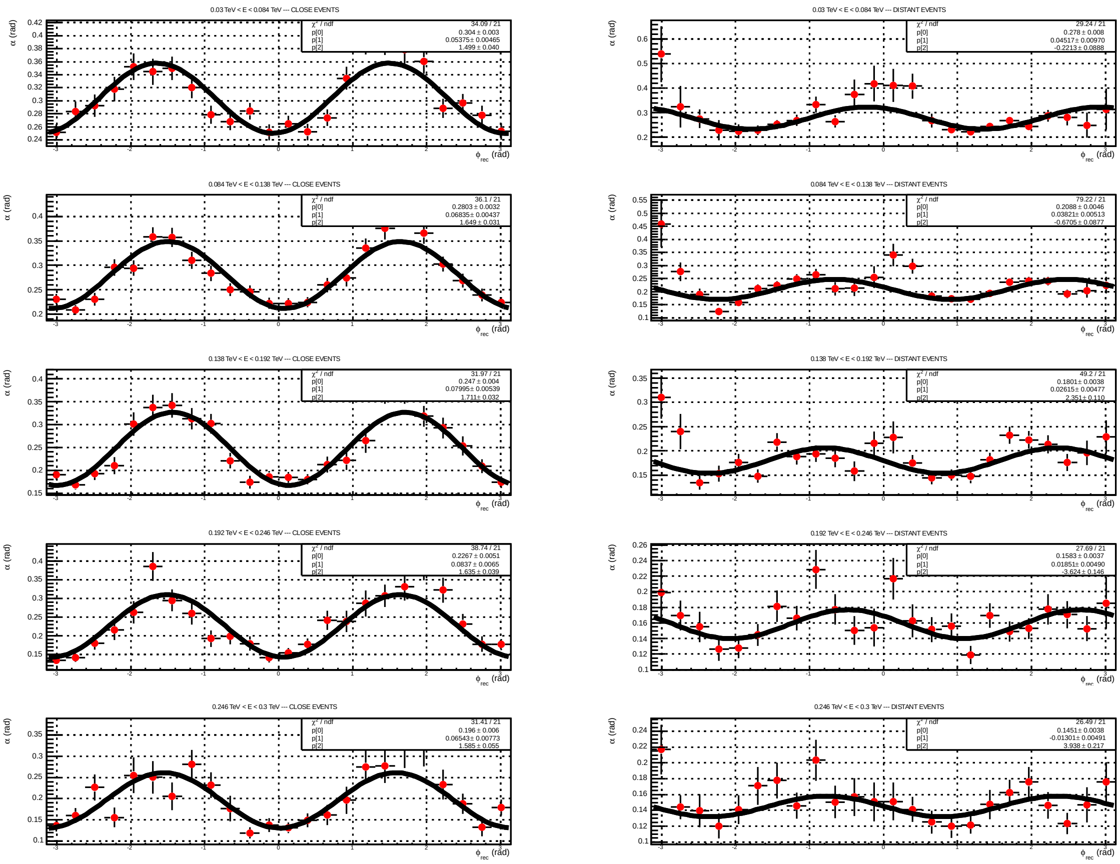

Figure 8: α-distribution plots for different energy ranges; the left plots show the nearby events ($dp < 200\ m$) distribution and the right plots show the distant events ($dp > 200\ m$) distribution.

Obviously, if the geomagnetic field produces a distorsion in the shape and in the direction of individual images, it will also affect the reconstructed source position and hence the angular resolution. To get an improved angular resolution, one should be able

[5]i.e. after removing pixels with charges smaller than a pre-defined threshold which is sufficiently high to retain the shower contribution and suppress the NSB.

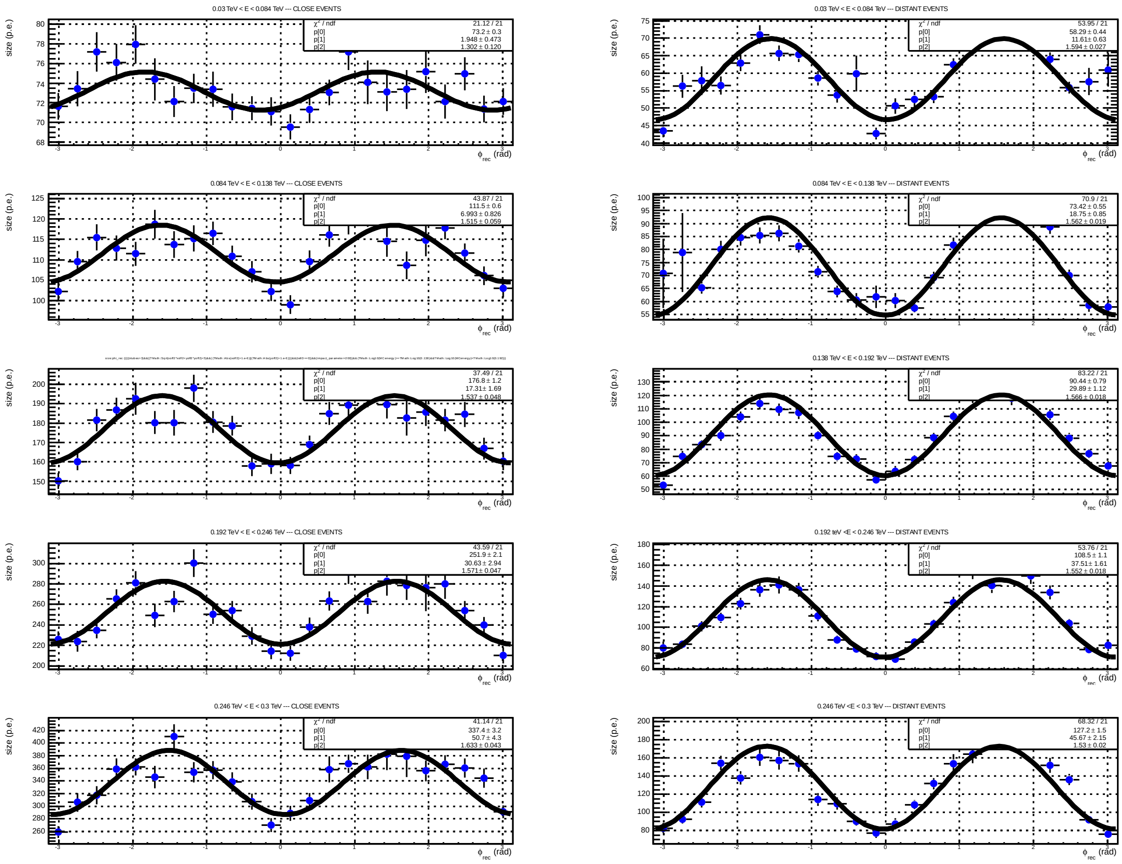

Figure 9: *size*-distribution plots for different energy ranges; the left plots show the nearby events ($dp < 200\ m$) distribution and the right plots show the distant events ($dp > 200\ m$) distribution.

to evaluate the amount of the distorsion due to the geomagnetic field in order to apply the appropriate corrections.

As we discussed before in the case of α and *size* distributions, the geomagnetic field effect on these parameters varies with the energy and with the distance from the telescopes. For this reason the correction to be applied on each weight should be performed on the event basis.

In figure 8, 9, 10 and 11 are respectively shown α-plots (red markers), *size*-plots (blue markers), *length*-plots (green markers) and *width*-plots (yellow markers) as a function of the azimuth angle ϕ_{rec} in the camera system. Each plot has been calculated for a different energy range; the full energy range has been divided in 5 intervals: $0.03\ TeV < \Delta E_1 < 0.084\ TeV$, $0.084\ TeV < \Delta E_2 < 0.138\ TeV$, $0.138\ TeV < \Delta E_3 < 0.192\ TeV$, $0.192\ TeV < \Delta E_4 < 0.246\ TeV$ and $0.246\ TeV < \Delta E_5 < 0.3\ TeV$. The left plots show the nearby events distributions and the right plots show the distant events distributions. Each image parameter has a characteristic modulation shape for a fixed combination of energy and impact parameter. In order to improve the angular resolution, we will evaluate the correction to apply to these image parameters for individual events.

The reference value for null geomagnetic field intensity corresponds to the average value $p[0]$ of each distribution. This can be explained by the opposite effect of the geomagnetic field between camera azimuth parallel and perpendicular to Lorentz force projection (see figure 4). At the same time, the phase of the modulation $p[2]$ is nearly constant. Starting

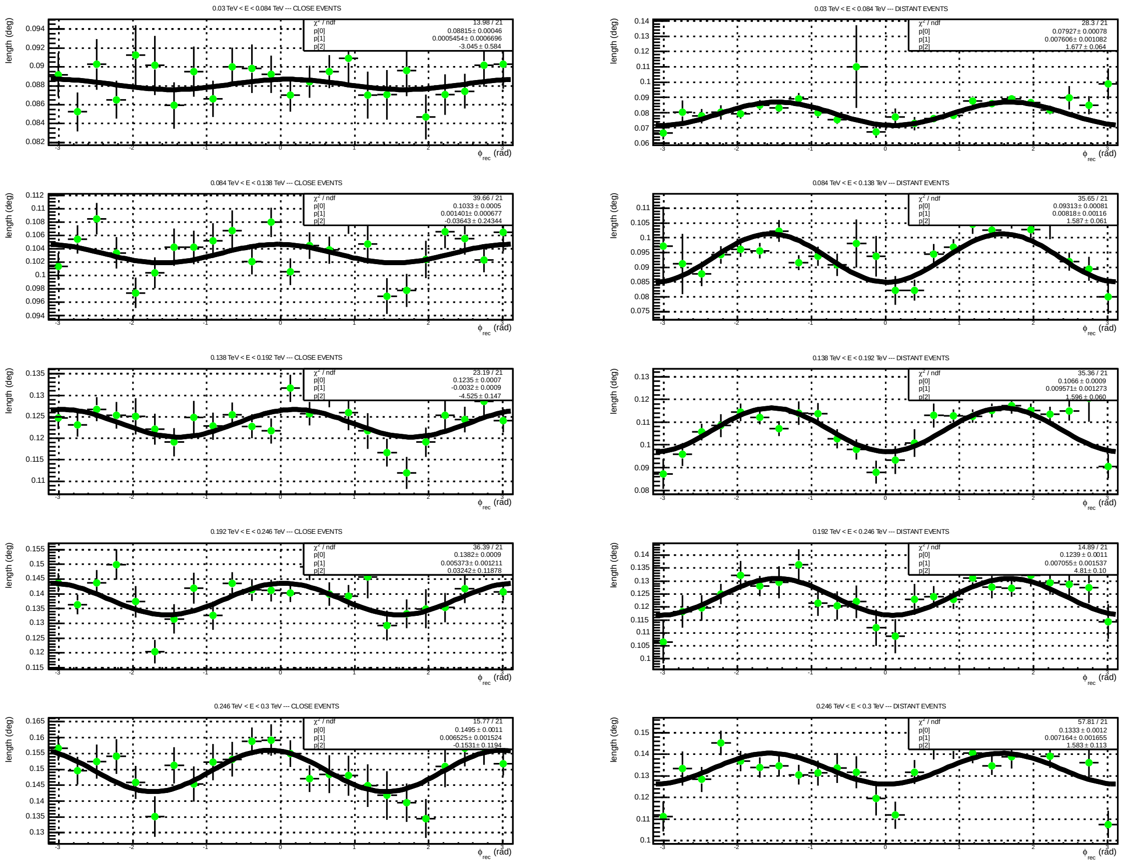

Figure 10: *length*-distribution plots for different energy ranges; the left plots show the nearby events ($dp < 200\ m$) distribution and the right plots show the distant events ($dp > 200\ m$) distribution.

from the knowledge of the parameters $p[0]$, $p[1]$ and $p[2]$ from the fitted distributions, we interpolated the value of each image variable (i.e. *alpha*, *size*, *length* and *width*) for every given ϕ_{rec} angle. In this way one can get the amount of distorsion due to the geomagnetic field with respect to the corresponding average value $p[0]$. In this way we obtained a full parametrization of the geomagnetic field effect as a function of azimuth angle ϕ_{rec}, energy E and impact parameter dp.

After correcting *alpha*, *size*, *length* and *width*, new weights can be used to reconstruct the source position. We expect that the width of the distribution of the reconstructed positions after the correction to the image parameters will be narrower, and the corresponding angular resolution will be smaller.

5 CONCLUSION

The Earth's magnetic field deflects charged particles in the extensive air showers. Consequently, the Cherenkov light images in the camera of an IACT are rotated and modified in size. This phenomenon adds up to other effects that degrade the angular resolution of the Cherenkov telescopes, such as the fluctuations of the first interaction depth of primary particles, shower fluctuations or the finite number of pixels used for reconstruction. In this work, we proposed a method to correct for the geomagnetic field effect. We implemented

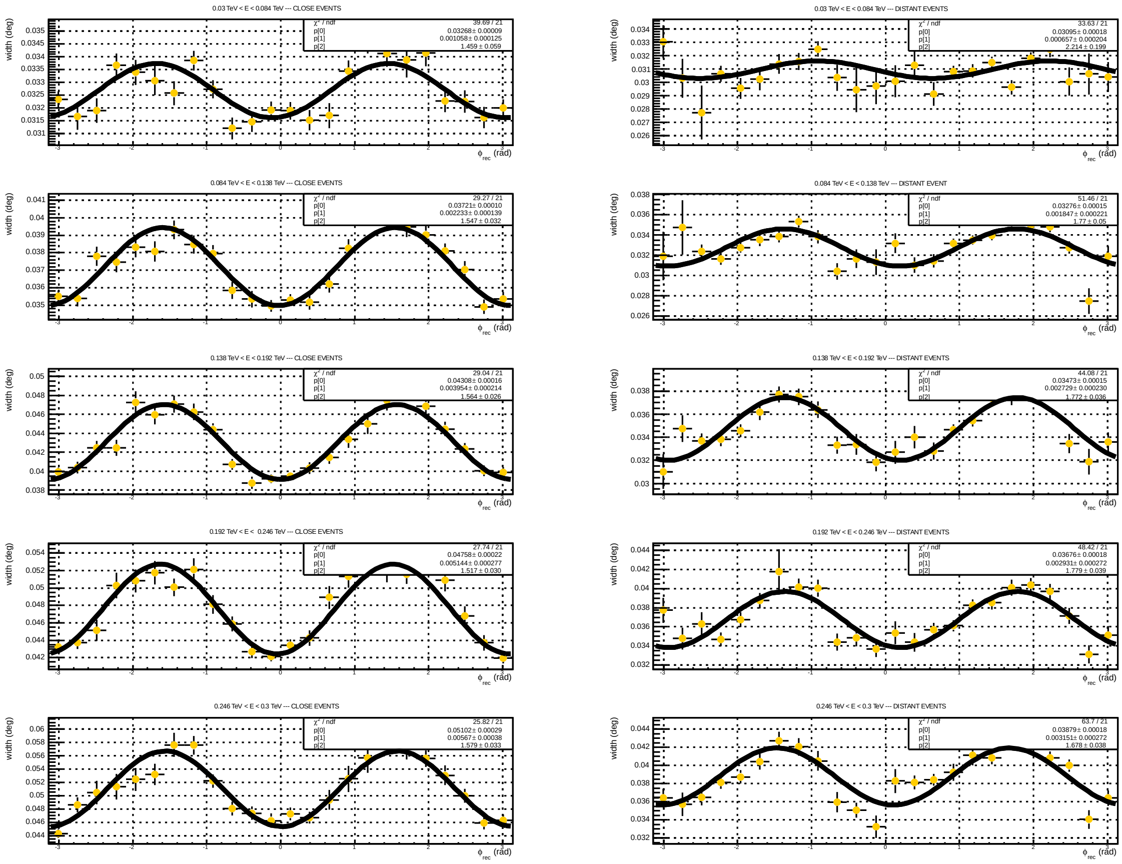

Figure 11: *width*-distribution plots for different energy ranges; the left plots show the nearby events ($dp < 200\ m$) distribution and the right plots show the distant events ($dp > 200\ m$) distribution.

the full parameterisation of the modulation of the image parameters as a function of the azimuth in the IACT camera, and for different energies and impact parameters. This study has allowed us to define the parameter space regions important for angular and energy resolution of arrays of IACTs.

To reconstruct the source position of array events, a weighting procedure which makes use of the orientation, light density and shape of individual telescope images, is employed. We have shown that these parameters are all affected by the geomagnetic field and need different correction to be applied in order to minimize the impact on the angular resolution. Interpolating the parametrization of the geomagnetic modulation for invidual images, we have been able to quantify the amount of correction to be applied. The implementation of the correction is in progress and will make use of the obtained results as a main input.

Acknowledgments

I would like to express all my gratitude to my supervisor Serguei Vorobiov for his essential help, his precious advises and his patience. Many thanks. I want to thank all the people working at the CTA Group in DESY and all the ones involved in the organization of this Summer Student Programme: it was a great experience, I learnt a lot. A special thank to my friends Laura and Stefania for their support. Thanks for making me feel at home.

References

[1] K. Nakamura et al. (Particle Data Group), J. Phys. G 37, 075021 (2010).

[2] J.A. Hinton and W. Hofmann, *Teraelectronvolt Astronomy*, arXiv:1006.5210v2 [astro-ph.HE] (2010).

[3] F. Aharonian et al. *High energy astrophysics with ground-based gamma ray detectors*, Rep. Prog. Phys. 71 096901 (2008).

[4] W.R. Leo, *Techniques for Nuclear and Particle Physics Experiments*, Springer-Verlag (1994).

[5] T. Stanev, *High Energy Cosmic Rays*, Springer (2010).

[6] S.C. Commichau et al. *Monte Carlo studies of geomagnetic field effects on the imaging air Cherenkov technique for the MAGIC telescope site*, Nuclear Instruments and Methods in Physics Research A 595 (2009).

[7] P.M. Chadwick et al., *The correction of atmospheric Cherenkov images for the effect of the geomagnetic field*, J. Phys. G: Nucl. Part. Phys. 26 (2000).

[8] M. Krause, *Studies of the influence of the geomagnetic field on the sensitivity of gamma-ray observatories*, Bachelor Thesis (2011).

[9] S. Vorobiov, *Observations of the Crab Nebula from 1996 to 2002 by the atmospheric Cherenkov telescope CAT and implementation of a new analysis method applicable to atmospheric showers*, PhD. Thesis (2004).

[10] W. Hofmann et al. *Comparison of techinques to reconstruct VHE gamma-ray showers from multiple stereoscopic Cherenkov images*, Astroparticle Physics (1999).

[11] Cherenkov Telescope Array, http://www.cta-observatory.org/

[12] DESY Zeuthen - CTA group, http://nuastro-zeuthen.desy.de/cta/

[13] National Geographic Data Center (NGDC), http://www.ngdc.noaa.gov/geomag/